Highly sensitive ultraviolet sensor based on ZnO nanorod film deposited on ST-cut quartz surface acoustic wave devices

W. Li[a,b], Y. J. Guo[a,*], Q. B. Tang[a], X. T. Zu[a], J. Y. Ma[c], L. Wang[c], K. Tao[d], H. Torun[e], Y. Q. Fu[e,*]

[a] School of Physics, University of Electronic Science and Technology of China, Chengdu, 610054, People's Republic of China

[b] School of Chemistry, Physics and Mechanical Engineering, Queensland University of Technology, Brisbane, Queensland 4001, Australia

[c] Sichuan Institute of Piezoelectric and Acousto-Optic Technology, Chongqing 400060, People's Republic of China

[d] Ministry of Education Key Laboratory of Micro and Nano Systems for Aerospace, Northwestern Polytechnical University, Xi'an 710072, PR China

[e] Faculty of Engineering & Environment, University of Northumbria, Newcastle upon Tyne, NE1 8ST, UK

Abstract: A highly sensitive surface acoustic wave (SAW) ultraviolet (UV) detector operated at room temperature was developed using a sensing layer of zinc oxide (ZnO) nanorods (NRs) grown on ST-cut quartz using a hydrothermal method. Under illumination of the UV light with a wavelength of 365 nm and an intensity of 6 μW cm^{-2}, the resonant frequency of the SAW UV sensor based on ZnO NRs/ZnO nanofilm structure was decreased by ~200 Hz, mainly due to electroacoustic effect. NR structures enhance the sensitivity of the sensor. The estimated enhancement in the sensitivity based on the experimental results is ~3.5 folds compared to a device with only a thin

nanolayer ZnO film. Meanwhile, density of ZnO NRs over the ZnO seed layer was also investigated and an optimum design was proposed.

Keywords: SAW device; UV detector; ZnO nanorods;ST-cut quartz

*Corresponding authors
E-mail address:
Prof. Yuanjun Guo, guoyuanjun@uestc.edu.cn, Prof. Richard Yongqing Fu, richard.fu@northumbria.ac.uk

1. Introduction

In recent years, ultraviolet (UV) light detection has gained much more attention from scientists and researchers for various applications, such as chemical and biological processes [1,2], flame detection [3], astronomy and aerospace [4,5]. Zinc oxide (ZnO) is a commonly used optoelectronic material with a wide band gap of 3.4 eV and a large exciton binding energy of 60 meV at room temperature [6]. In addition, ZnO layers can be deposited using standard microfabrication methods. Therefore, it has been widely used in UV detectors, including metal-semiconductor-metal photo-transistors, photo-diodes, and surface acoustic wave (SAW) based photodetectors [7-9]. Among these devices, SAW sensors have many technical advantages including high sensitivity and fast response. In addition, they have practical advantages, as they are easy to manufacture and are suitable for remote and wireless operations [10,11].

However, many piezoelectric SAW sensors are prone to variations in temperature [12]. Among the commonly used piezoelectric substrates, ST-cut quartz has the lowest temperature coefficient of frequency (TCF) [13, 14], thus is an ideal substrate for fabricating SAW devices.

Recently, nanostructures have been demonstrated to enhance the sensing performance of piezoelectric sensors. Among various ZnO nanostructures, ZnO nanorods (NRs) have wide-range applications in solar cells, biosensors, nano-generators, UV detectors, and humidity sensing, due to their large ratio to surface area vs volume [15–19].

Although various ZnO-based UV light sensors have been developed [7,20-27], to our knowledge, the concept of UV sensing based on ST-cut quartz SAW devices coated with ZnO NRs has not been fully explored. In this work, we have systematically explored ZnO NRs on ST-cut quartz SAW devices for UV sensing **via the different densities of NRs from 0 (nanofilm) to 100%**. We have fabricated devices on ST-cut quartz substrates and experimentally characterized their performance especially with an emphasis on the evaluation of density of ZnO NRs over the ZnO seed layers. Density refers to the ratio of the ZnO NRs area projected over the sensor surface to the area of ZnO seed layer. We identified the importance of this parameter for UV sensing.

2. Experimental

A schematic diagram of the UV measurement system is shown in Fig. 1 (a). The SAW sensor is based on an oscillator which consists of a sensing film coated SAW resonator device with its corresponding amplifying and phase-shift circuits. The output signal of the SAW sensor was measured using a frequency counter (Agilent 53210). The two-

port SAW resonator was fabricated on an ST-cut (42°75′) quartz using a conventional photolithography and lift-off process. The process parameters of the SAW device, employing an interdigital transducer (IDT) made of aluminum with a thickness of 200nm are summarized in Table 1. A schecmatic diagram with the size details of the SAW device is shown in Fig. 1(b). A network analyzer (Hewlett Packard 8714C) was used to measure the characteristics of the SAW devices.

ZnO nanolayer films with a thickness of 30 nm were deposited onto the surface of the SAW device using a combined sol–gel and spin-coating process. Zinc acetate dehydrate ($Zn(CH_3COO)_2 \cdot 2H_2O$) was dissolved into a 2-methoxyethanol–monoethanolamine (MEA) solution and then used in the spin-coating process. During the spin-coating, a ZnO nanofilm with a thickness of 30 nm was prepared on the surface of the SAW devices at a speed of 3000 rpm for 30 s. Then, the coated SAW devices were directly transferred into the furnace to be kept at 300 ◦C for 10 min, followed by annealing at a temperature of 500 ◦C for 1 h [28, 29]. ZnO NRs were then grown on the above seed-layer of ZnO film using a low temperature hydrothermal method with chemicals of zinc nitrate hexahydrate ($Zn(NO_3)_2 \bullet 6H_2O$) and methenamine ($C_6H_{12}N_4$), which concentrations in the solution were both 10 mmol/L. The device was floated on the surface of the solution to grow the NRs at 90° for 150 mins. During the process, the SAW device was facing down and its IDTs were protected with polyimide tape. After growth, the polyimide tape was removed and the device was washed three times by ethanol and di-water before heating at 60°C for 300 mins in a thermostatic drying oven. During the process, the IDTs of the SAW device was protected with polyimide tape. In addition, polyimide tape was also used as a physical control agent for the growth of ZnO NRs over the ZnO seed layer. The density of ZnO NRs over the ZnO seed layer

on ST-cut quartz SAW device was varied as 35%, 60%, and 100%. These metrics correspond to areal coverage. After the growth, the SAW device was rinsed with deionized water to remove the residual materials and dried for further characterization. The ZnO NRs were also grown on glass in order to characterize the optical properties of the ZnO films and NRs.

A field-emission scanning electron microscope (FE-SEM, Carl Zeiss 1530 VP) and an atomic force microscope (AFM, Being technology 5500) were used to characterize morphologies of the ZnO nanofilm and ZnO NRs. In addition, a UV-VIS spectrophotometer (UV-2550, Shimadzu) was used to characterize the optical transmission properties of the samples of ZnO nanofilm/glass and ZnO NRs/ ZnO nanofilm/glass. The crystallinity of the prepared ZnO nanofilm and ZnO NRs were characterized using an X-ray diffraction (XRD) analysis (Rigaku D/max-2400 X-ray diffractometer). For the UV sensing experiments, a portable UV Analyzer (CBIO-UV2A, Beijing CBIO Bioscience & Technologies) was used as a UV source (with a wavelength of 365 nm) and a UV intensity meter (LS126A, Linshang, China) was used to detect the intensity.

3. Results and discussion

Fig. 2 shows a top-view SEM image of a typical ZnO nanofilm. The ZnO film is relatively smooth with an average size of nanoparticles in the range of 20-50 nm. Fig. 3 shows an AFM image of ZnO nanofilm, where the surface roughness of the film is ~3.84 nm.

Fig. 4 shows the transmission S_{12} signal of the SAW devices with varying density of

ZnO NRs. When the density of ZnO NRs is increased from 35% to 100%, the center frequency is decreased from 200.02 MHz to 199.55 MHz, and the insertion loss is decreased from -15.9 dB to -33.0 dB. The devices with smaller insertion losses operate more effectively in our experimental setup shown in Fig. 1 considering the detection limits of the frequency counter and the characteristics of the amplifiers. As mentioned above, a SAW sensor is based on an oscillator which consists of a sensing film coated onto a SAW resonator device, and also amplifying and phase-shift circuits as shown in Fig.1 (a). We found that the device could not work properly when the insertion loss of the signal is less than – 30 dB. From Fig. 4, we can see the insertion loss decreases under -30 dB when the density of NRs is larger than 35%. Consequently, we chose the SAW device with a ZnO NRs density of 35% for UV sensing.

Fig. 5(a) and (b) shows a top-view and a cross-section of SEM images of ZnO NRs on top of the SAW device, and the ZnO NRs are densely packed with uniform coverage. The diameters and lengths of ZnO NRs are in the range of 50-100 nm and 300-500 nm, respectively.

Fig. 6 shows the XRD patterns of the ZnO-nanofilm/glass sample and ZnO-NRs/ZnO-nanofilm/glass sample，respectively. The XRD pattern of the ZnO nanofilm shows weak peaks within a broad background due to its thickness of only 30 nm on the amorphous feature of glass substrate. The characteristic XRD peaks of ZnO NRs are at 31.76° and 34.49°, which correspond to the (10-10) and (0002) planes of ZnO, respectively. The peak at (0002) shows a higher relative intensity than that of the peak at (10-10), which indicates that the ZnO NRs have a preferred orientation along (0002) direction.

Fig. 7 comparatively shows the optical transmission signals of the ZnO-NRs/ZnO-nanofilm/glass and ZnO-nanofilm/glass samples. The transmittance of the former is lower within a spectral range of 265-800 nm. Furthermore, we also calculated the absorbance values of the two samples to the UV light with a wavelength of 365 nm according to the relationship between absorbance and transmittance A= -lg(T). The absorbance of ZnO-NRs/ZnO-nanofilm/glass sample was ~0.356 whereas that of ZnO-nanofilm/glass was ~0.189 which indicates that ZnO NRs layer absorbed more UV light than the thin ZnO film layer.

Fig. 8 shows the dynamic response characteristics of the sensors with ZnO nanofilm and ZnO NRs (with the NRs density of 35%). We used a calibrated UV light source with a wavelength of 365 nm and a power density of 24 $\mu W/cm^2$. Both sensors were responsive well to the UV light. The sensor based on ZnO NRs has a negative response about -687 Hz, whereas that based on ZnO nanofilm has a negative response of -223 Hz. The frequency shift of the sensor based on the ZnO NRs is about 3 times larger compared with the sensor based on ZnO nanofilm. However, the same experiment revealed that the recovery time for the sensor based on ZnO NRs is quite long, compared with that using the sensor based on ZnO nanofilm. Qualitatively, the recombination of photon-generated carriers has two different mechanisms. One is the bulk recombination inside the ZnO microstructures, which is fast. The other is the surface recombination caused by the adsorbed oxygen at the surface of the ZnO, which is slow. ZnO NRs devices consisting of both nanofilm and NRs on top of the film have a much larger surface than that of the nanofilm based devices, therefore the recombination with the absorbed oxygen on the surface of NRs will take much longer

time, resulting in a much longer response time [30].

The UV detection mechanism of SAW devices is associated with the adsorption and desorption of oxygen molecules from the sensing layer [31]. Before the sample was irradiated to the UV light, oxygen molecules are adsorbed on the surface of ZnO layer and will capture the free electrons on the surface. The reactions are shown in the equations:

$$O_2(g) + e^- \rightarrow O_2^-(ad) \quad (1.1)$$

$$O_2(g) + 2e^- \rightarrow O_2^{2-}(ad) \quad (1.2)$$

This will decrease the charge carrier density and the mobility of the charges. As a result, a depletion layer with a low conductivity is formed near the surface of ZnO layer. When the sensor is exposed to the UV light, electron–hole pairs will be quickly generated. The holes will migrate to the surface as the electric field is generated in the depletion region, and they will recombine with the adsorbed oxygen ions through surface recombinations, thus releasing oxygen molecules from the surface. These processes can be written as follows:

$$O_2^-(ad) + h^+ \rightarrow O_2\ (g) \quad (2.1)$$

$$O_2^{2-}(ad) + 2h^+ \rightarrow O_2(g) \quad (2.2)$$

The unpaired electrons will significantly enhance the conductivity of ZnO layer. Due to the enhanced UV absorption and a large ratio of surface area/volume, the sensing layer of ZnO NRs generates more electron–hole pairs than the ZnO nanofilm layer does under identical UV illumination conditions. Therefore, the increase in conductivity for the ZnO NRs based device is much larger than that in the ZnO nanofilm device.

Changes in the center frequency of the SAW devices during sensing can be attributed to various reasons such as mass loading, electroacoustic effect (electrical loading), and elastic loading [32]. Under UV radiation, the changes in the electrical properties (in

particular, conductivity and dielectric constant) of a thin film result in changes in the speed of sound, known as electroacoustic effect. The relationship between the change in SAW velocity (Δv) versus the sheet conductivity (σ_s) of the film can be described as [33, 34],

$$\frac{\Delta v}{v_0} \approx -\frac{K^2}{2}\frac{\sigma_s^2}{\sigma_s^2 + v_0^2 C_s^2} \quad (3)$$

where C_s is the surface capacity, σ_s is the sheet conductivity, K^2 is the electromechanical coefficient, v_0 is the unperturbed SAW velocity. Based on Eq. (3), when the sensor is exposed to UV light, the increase in the conductivity of the sensing layer (σ_s) will decrease SAW velocity. Hence, the resonant frequency will decrease. In this paper, we investigated the enhancement effect of ZnO NRs grown on the ZnO nanofilm layer. Additional electrons generated in the NRs will be transported quickly to the seed layer, thereby increasing the conductivity of the device. This is the main mechanism for larger frequency shifts that we systematically observed in this study.

Figs. 9(a) and 9(b) show the cyclic response of the sensors based on both the ZnO NRs and ZnO nanofilm. We exposed the devices to a 24 μW/cm^2 UV light for 4 cycles. The obtained sensing performance parameters are listed in Table 2. The average frequency shift of the sensors with ZnO NRs is -671 Hz, with a maximum variance of 3%. Whereas for sensors with ZnO nanofilm, the average frequency shift is -236 Hz, with a variance of 5%. Results indicate better reproducibility for SAW devices with ZnO NRs.

Frequency responses of the SAW UV sensors based on ZnO NRs and ZnO nanofilm exposed to different power densities of the UV light are shown in Figs. 9(c) and 9(d), respectively. The sensing parameters are summarized in Table 3. The frequency shifts of the sensor based on ZnO NRs are much larger than those of the sensor with ZnO

nanofilm at all different UV light intensities. Even under a low intensity UV irradiation of 6 μW/cm^2, the response of the sensor based on ZnO NRs is 1.6 times higher than that of the sensor based on ZnO nanofilm.

The response time of both sensors tends to be smaller under lower UV illumination levels from 6 μW/cm^2 to 36 μW/cm^2. However, the response time with ZnO NRs under a 48 μw/cm^2 UV irradiation is 450 s, which is smaller than that (536 s) under a 36 μW/cm^2 UV irradiation, and the sensor with ZnO nanofilm has similar results. According to the slopes of curves shown in Figs. 9(c) and 9(d), the speed of response becomes slower with lower UV irradiation intensity. Sensors will respond faster under higher intensity UV irradiation, but the peak response (amplitude of frequency shift) of sensors is smaller under a lower intensity UV irradiation. Therefore, there should be a threshold intensity. Sensors will respond quickly at a faster speed to get the amplitude of frequency shift under a higher intensity UV irradiation than the threshold intensity. When the intensity of UV irradiation is below this threshold, the response would be slower; however, it is easier for the sensors to reach the peak response because of the small amplitude of frequency shift. In this paper, the threshold UV irradiation intensity was identified to be between 36 μW/cm^2 and 48 μW/cm^2.

Fig. 10 shows that the frequency shift of sensor with ZnO nanofilm has a linear relationship with UV intensity, which can be given as,

$$\Delta f_{nanofilm} = -4.7 \times \mathrm{I}_{\mu v} - 99.5 \ \ (Hz) \qquad (4)$$

where Δf is the frequency shift, $\mathrm{I}_{\mu v}$ is the UV intensity. Similarly, the relationship between the frequency shift and UV intensity for the SAW sensor with the ZnO NRs is given as,

$$\Delta f_{NRs} = -15.7 \times \mathrm{I}_{\mu v} - 195.5 \ \ (Hz) \qquad (5)$$

From the Eq. (4) and Eq. (5), it is obvious that the slope of Eq. (5) is 3.36 times as much as that of Eq. (4). It indicates that the response of the sensor with ZnO NRs is 3.36 times as high as that of the sensor based on ZnO nanofilm with the increase of UV intensity.

Table 4 summarizes the results of a few reported SAW UV detectors with ZnO as the sensing material obtained from literature [7, 24, 25, 27] and also from this study. The UV light sensitivity of the SAW devices is defined as,

$$S_{UV} = \frac{1}{f_r}\frac{\Delta f}{\Delta I_{UV}} \qquad (6)$$

where Δf is the frequency shift of SAW devices, f_r is the resonant frequency, and ΔI_{UV} is the change of UV light intensity. Compared with all the other calculated sensitivity results listed in Table 4, the UV sensitivity of ZnO NRs based SAW devices in this work is comparable, e.g., 93.7 ppm $(mW/cm^2)^{-1}$. It should be pointed out that the different sensitivities and frequency shifts are significantly influenced by the growth substrate, deposition conditions of ZnO sensing layer, intrinsic resonant frequency of the device, SAW vibration mode, and UV intensity, et al.

4. Conclusions

In general, a SAW sensor consists of a sensing structure coated onto the SAW resonator device with its corresponding amplifying and phase-shift circuits. The ZnO structures work as the sensing structure in the device. ZnO structure work to detect the changes and response to targeted detections via producing some impact on the surface wave of SAW device. In this work, we fabricated a UV detector based on ST-cut quartz SAW devices using hydrothermally grown ZnO NRs. In addition, we fabricated another SAW-based UV detector with a ZnO nanofilm using a combined sol–gel and spin-

coating process for comparison purposes. We varied the density of NRs over the seed layer to optimize the device for UV sensing. We experimentally validated that a density of 35% is optimum. The SAW device with the ZnO NRs showed enhanced absorbance for 365 nm UV light compared with that made of the ZnO nanofilm. The sensor is sensitive even under low-level UV illumination. Under a low UV light intensity of 6 $\mu W\ cm^{-2}$, the frequency of the SAW UV sensor based on ZnO NRs/ZnO nanofilm structure decreases by ~200 Hz. Furthermore, under irradiation with different UV intensities, the sensor based on ZnO NRs showed a much higher UV light sensitivity than that based on the ZnO nanofilm (e.g., 93.7 versus 31.3 ppm/(mw/cm^2)). We experimentally obtained a linear response under UV illumination up to a level of 50 $\mu W/cm^2$.

Acknowledgment

The authors acknowledge the support by the National Natural Science Foundation of China (No. 11304032). Funding supports from UK Engineering Physics and Science Research Council (EPSRC EP/P018998/1), Newton Mobility Grant (IE161019) through Royal Society and NFSC, and Royal academy of Engineering UK-Research Exchange with China and India are also acknowledged.

References:

[1] A. Kolmakov, M. Moskovits, Chemical sensing and catalysis by one-dimensional metal-oxide nanostructures, Annu. Rev. Mater. Res. 34 (2004) 151-180.

[2] K. Saha, S. S. Agasti, C. Kim, X. Li, V. M. Rotello, Gold nanoparticles in chemical and biological sensing, Chem. Rev. 112 (2012) 2739-2779.

[3] E. Munoz, E. Monroy, J. L. Pau, F. Calle, F. Omnes, P. J. Gibart, III nitrides and

UV detection, Phys.: Condens. Matter. 13 (2001) 7115.

[4] C. L. Joseph, UV Image sensors and associated technologies, Exp. Astron. 6 (1995) 97-127.

[5] R. R. Meier, Ultraviolet spectroscopy and remote sensing of the upper atmosphere, Space Sci. Rev. 58 (1991) 1-185.

[6] Ü. Özgür, Y. I. Alivov, C, A. Teke, M. A. Reshchikov, S. Doğan ... H. Morkoç. A comprehensive review of ZnO materials and devices. *Journal of applied physics*, *98*(4) (2005), 11.

[7] D. T. Phan, G. S. Chung, Characteristics of SAW UV sensors based on a ZnO/Si structure using third harmonic mode, Curr. Appl. Phys. 12 (2012) 210-213.

[8] Y. Q. Fu, J. K. Luo, N. T. Nguyen, A. J. Walton, A. J. Flewitt, X. T Zu, Y. Li, G. McHale, A. Matthews, E. Iborra, H. Du, W.I. Milne, Advances in piezoelectric thin films for acoustic biosensors, acoustofluidics and lab-on-chip applications, Prog. Mater Sci. 89 (2017) 31-91.

[9] Y. Q. Fu, J. K. Luo, X. Du, A. J. Flewitt, Y. Li, A. Walton, W.I. Milne, Recent developments in ZnO films for acoustic wave based bio-sensing and microfluidic applications, Sens. Actuat. B. 143 (2010) 606-619.

[10] P. Sharma, S. Kumaral, K. Sreenivas, Interaction of surface acoustic waves and ultraviolet light in ZnO films, J. Mater. Res.18 (2003) 545-548.

[11] S. Y. Wang, Z. J. Li, X. S. Zhou, X. T. Zu, Y. Q. Fu, Advances in Nanostructured Acoustic Wave Technologies for Ultraviolet Sensing, Nanosci. Nanotechnol. Lett. 7 (2015) 169-192.

[12] W. Ma，W. Shi, Temperature-sensitive cuts for surface acoustic waves in quartz, IEEE Trans. Ultrason. Ferroelectr. Freq. Control, 48 (2001) 333-335.

[13] E. Henry-Briot，S. Ballandras，G. Marianneau，G. Martin, Influence of metal thickness on phase velocity and thermal sensitivity of SAW devices, IEEE Trans. Ultrason. Ferroelectr. Freq. Control, 48 (2001), 538-546.

[14] T. Yamazaki，K. Iizawa，S. Kanna，M. Takagi, Temperature stability of surface acoustic wave resonators on in-plane rotated 33° Y-cut Quartz, Jpn. J. Appl. Phys. 42 (2003), 3136-3138.

[15] Z. L. Wang, ZnO nanowire and nanobelt platform for nanotechnology, Materials Science & Engineering R Reports, 64 (2009), 33-71.

[16] I. Udom, M. K. Ram, E. K. Stefanakos, A. F. Hepp, D. Y. Goswami, One dimensional-ZnO nanostructures: Synthesis, properties and environmental applications. Materials Science in Semiconductor Processing, 16 (2013), 2070-2083.

[17] Y. Zhang, M. K. Ram, E. K. Stefanakos, D. Y. Goswami, Synthesis, characterization, and applications of ZnO nanowires, Journal of Nanomaterials 2012 (2012), 4661-4677.

[18] C. O. Chey, Z. H. Ibupoto, K. Khun, O. Nur, M. Willander, Indirect determination of mercury ion by inhibition of a glucose biosensor based on ZnO nanorods, Sensors 12 (2012) 15063-15077.

[19] Q. Yang, W. Wang, S. Xu, Z. L. Wang, Enhancing light emission of ZnO microwire-based diodes by piezo-phototronic effect, Nano Letters 11 (2011) 4012-4017.

[20] L. S. Vikas, K. A. Vanaja, P. P. Subha, M. K. Jayaraj, Fast UV sensing properties of n-ZnO nanorods/p-GaN heterojunction, Sensors & Actuators A Physical 242 (2016) 116-122.

[21] V. Postica, I. Hölken, V. Schneider, V. kaidas, O. Polonskyi, V. Cretu, I. Tiginyanu, F. Faupel, R. Adelung, O. Lupan, Multifunctional device based on ZnO:Fe nanostructured films with enhanced UV and ultra-fast ethanol vapour sensing, Materials Science in Semiconductor Processing 49 (2016) 20-33.

[22] E. G. Barbagiovanni, V. Strano, G. Franzò, S. Mirabella, The role of Zn vacancies in UV sensing with ZnO nanorods, Appl. Phys. Lett. 109 (2016) 10482.

[23] N. W. Emanetoglu, J. Zhu, Y. Chen, J. Zhong, Y. Chen, Y. Lu, Surface acoustic wave ultraviolet photodetectors using epitaxial ZnO multilayers grown on r-plane sapphire, Appl. Phys. Lett. 85 (2004) 3702.

[24] S. Kumar, G. H. Kim, K. Sreenivas, R. P. Tandon, ZnO based surface acoustic wave ultraviolet photo sensor, J. Electroceram. 22 (2009) 198–202.

[25] P. Sharma, K. Sreenivas, Highly sensitive ultraviolet detector based on ZnO/$LiNbO_3$ hybrid surface acoustic wave filter, Appl. Phys. Lett. 83 (2003) 3617–3619.

[26] H. F. Pang, Y. Q. Fu, Z. J Li., Y. F. Li, F. Placido, A. Walton, X. T. Zu, Love mode surface acoustic wave ultraviolet sensor using ZnO films deposited on 36° Y-cut $LiTaO_3$ Sensors Actuators A 193 (2013) 87–94.

[27] Y. J. Guo，C. Zhao，X. S. Zhou，Y. Li，X. T. Zu, D. Gibson, Y. Q. Fu, Ultraviolet sensing based on nanostructured ZnO/Si surface acoustic wave devices, Smart Mater. Struct. 24 (2015), 125015.

[28] Y. L. Tang, Z. J. Li, J. Y. Ma, Y. J. Guo, Y. Q. Fu, X. T. Zu, Ammonia gas sensors based on ZnO/SiO_2 bi-layer nanofilms on ST-cut quartz surface acoustic wave devices, Sens. Actuators B Chem. 201 (2014), 114-121.

[29] W. Li, Y. J. Guo, Y. L. Tang, X. T. Zu, J. Y. Ma, L. Wang, Y. Q. Fu, Room-Temperature Ammonia Sensor Based on ZnO Nanorods Deposited on ST-Cut Quartz Surface Acoustic Wave Devices, Sensors, 17 (2017) 1142.

[30] W. Peng, Y. He, C. Wen, K. Ma, .Surface acoustic wave ultraviolet detector based on zinc oxide nanowire sensing layer. *Sensors and Actuators A: Physical.*（2012），*184*, 34-40.

[31] C. Soci, A. Zhang, B. Xiang, S. A. Dayeh, D. P. R. Aplin, J. Park, X. Y. Bao, Y. H. Lo, D. Wang, ZnO nanowire UV photodetectors with high internal gain. Nano letters, 7 (2007) 1003-1009.

[32] W.P. Jakubik, Surface acoustic wave-based gas sensors, Thin Solid Films, 520 (2011) 986-93.

[33] A. J. Ricco, S. J. Martin, T. E. Zipperian, Surface acoustic wave gas sensor based on film conductivity changes, Sensors and Actuators, 8 (1985) 319-333.

[34] W. Jakubik, Theory of SAW gas sensor based on bi-layer conductivity changes, Procedia Engineering 47 (2012) 1287-1290.

Fig.1 a) Schematic illustration of UV sensing set-up, b) schematic with size details of the SAW device.

Fig. 2 Top-view SEM image of ZnO nanofilm showing the surface features and nanoparticles.

Fig. 3 AFM image of the ZnO nanofilm.

Fig. 4 Transmission S_{12} signal of SAW devices with different density of ZnO NRs.

Fig. 5 a) Top-view and b) cross-section of SEM images of ZnO NRs on top of the SAW device.

Fig. 6 XRD patterns of ZnO-NRs/ZnO-nanofilm/glass and ZnO-nanofilm/glass

samples.

Fig.7 Optical transmission spectra of ZnO-NRs/ZnO-nanofilm/glass and ZnO-nanofilm/glass samples.

Fig. 8 Dynamic response characteristics of SAW sensors with ZnO nanofilm and ZnO NRs to the 365 nm UV light at a power density of 24 $\mu W/cm^2$.

Fig. 9 Frequency responses of SAW sensors based on (a) ZnO NRs and (b) ZnO nanofilm to 365 nm UV light at a power density of 24 $\mu W/cm^2$ for four cyclic irradiations; Frequency response of SAW sensors based on (c) ZnO NRs and (d) ZnO nanofilm to 365 nm UV light at different intensities.

Fig.10 Frequency shift of SAW sensors based on ZnO nanofilm and ZnO NRs as a function of UV intensity.

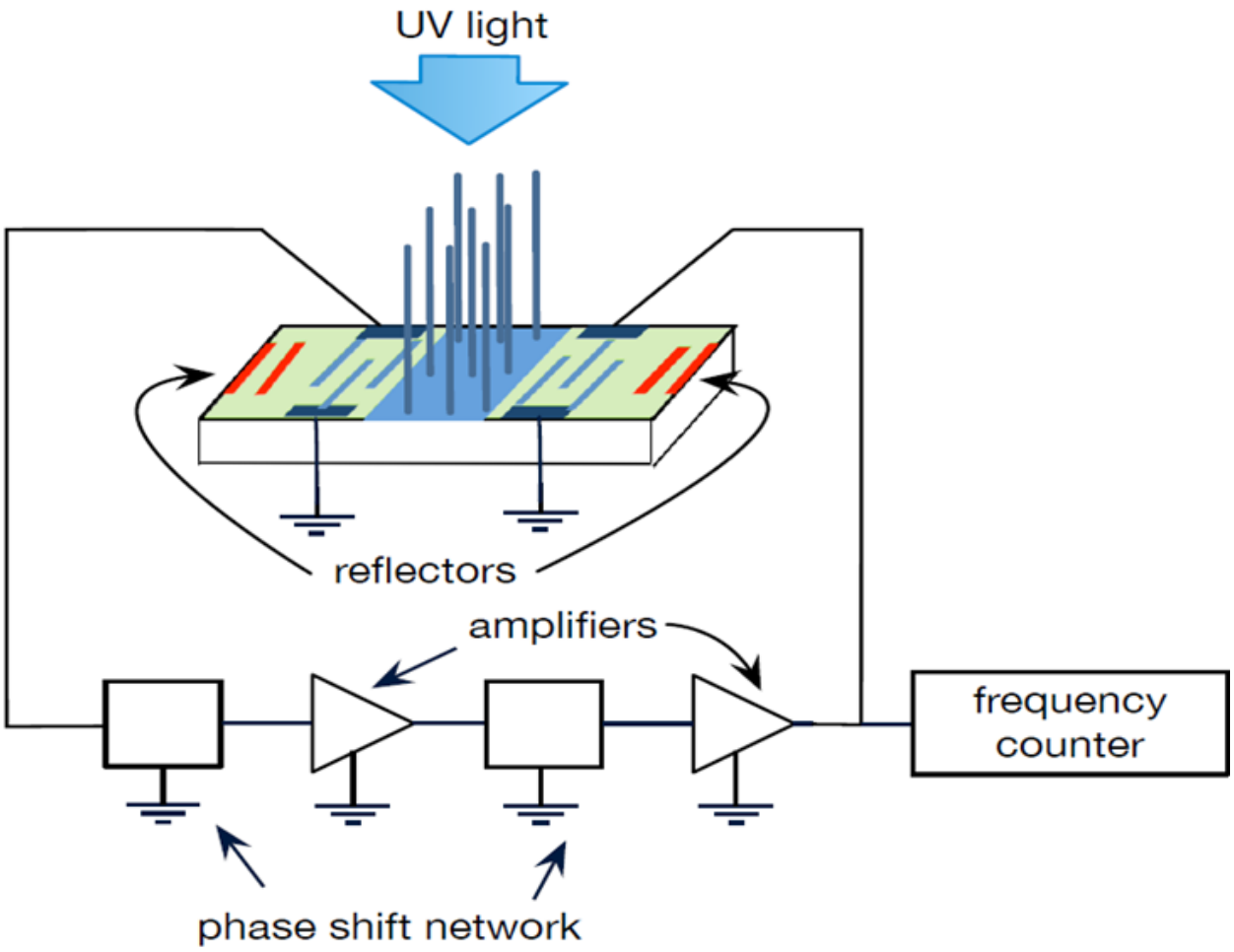
UV light
reflectors
amplifiers
frequency counter
phase shift network

(a)

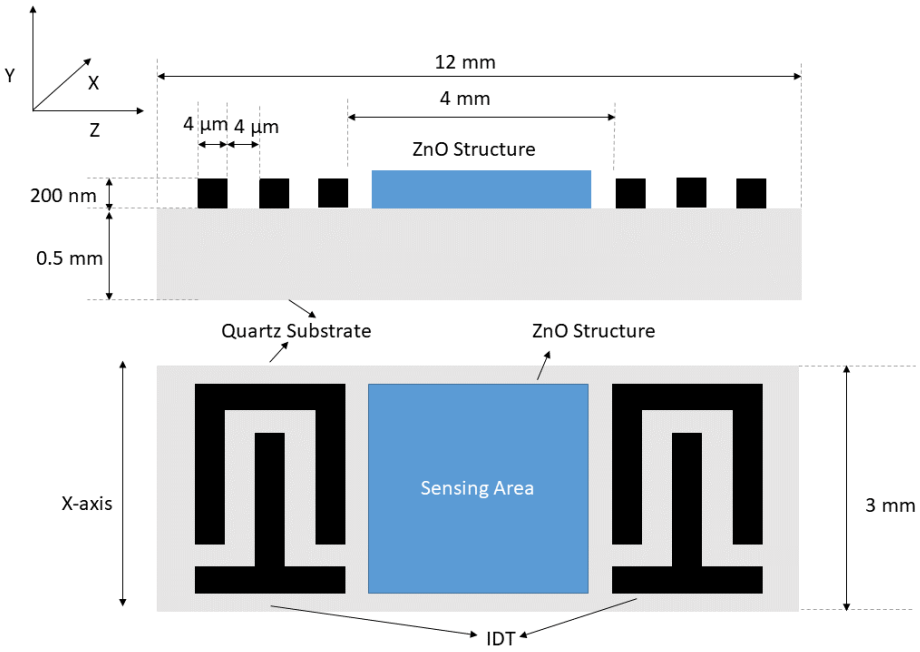
Y
X
Z
12 mm
4 mm
4 µm
4 µm
ZnO Structure
200 nm
0.5 mm
Quartz Substrate
ZnO Structure
X-axis
Sensing Area
3 mm
IDT

(b)

Fig.1

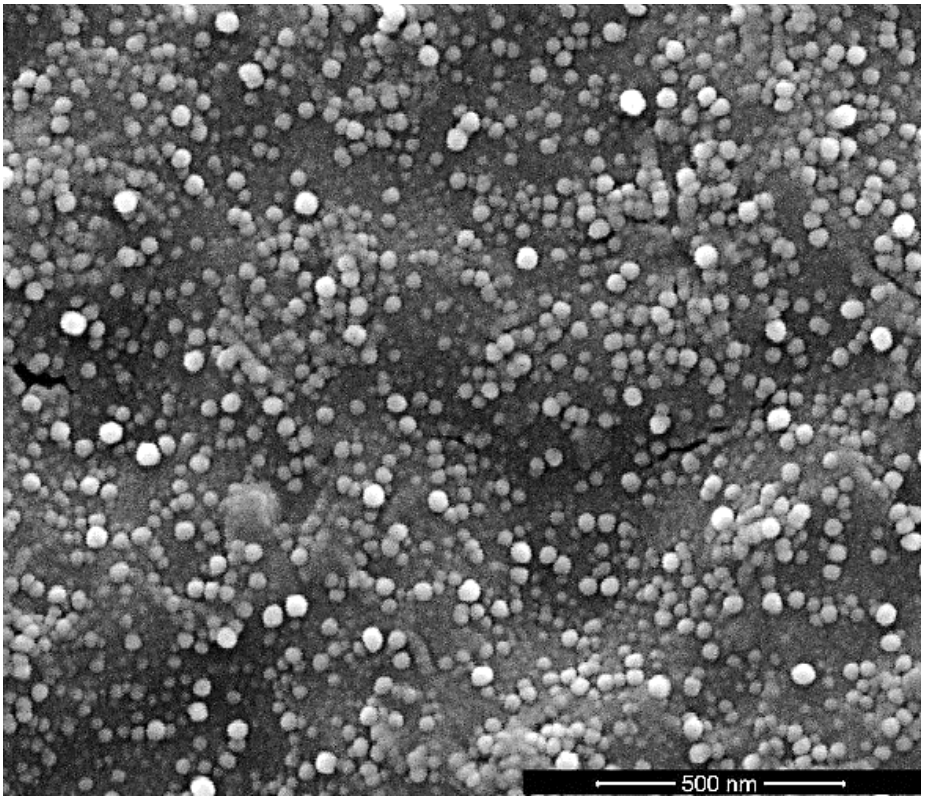

Fig.2

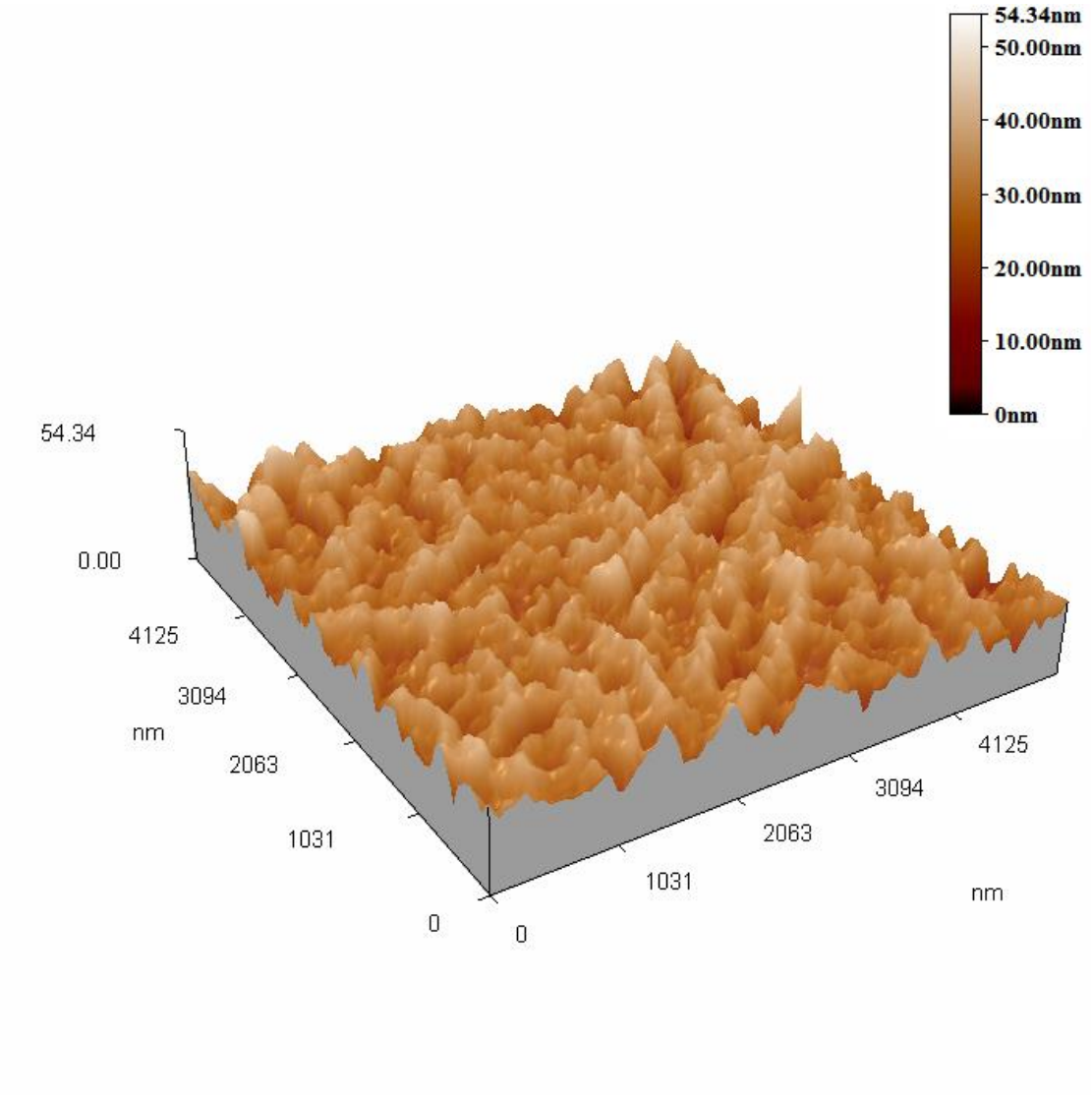
54.34nm
50.00nm
40.00nm
30.00nm
20.00nm
10.00nm
0nm
54.34
0.00
4125
3094
nm
2063
1031
0
0
1031
2063
3094
4125
nm

Fig.3

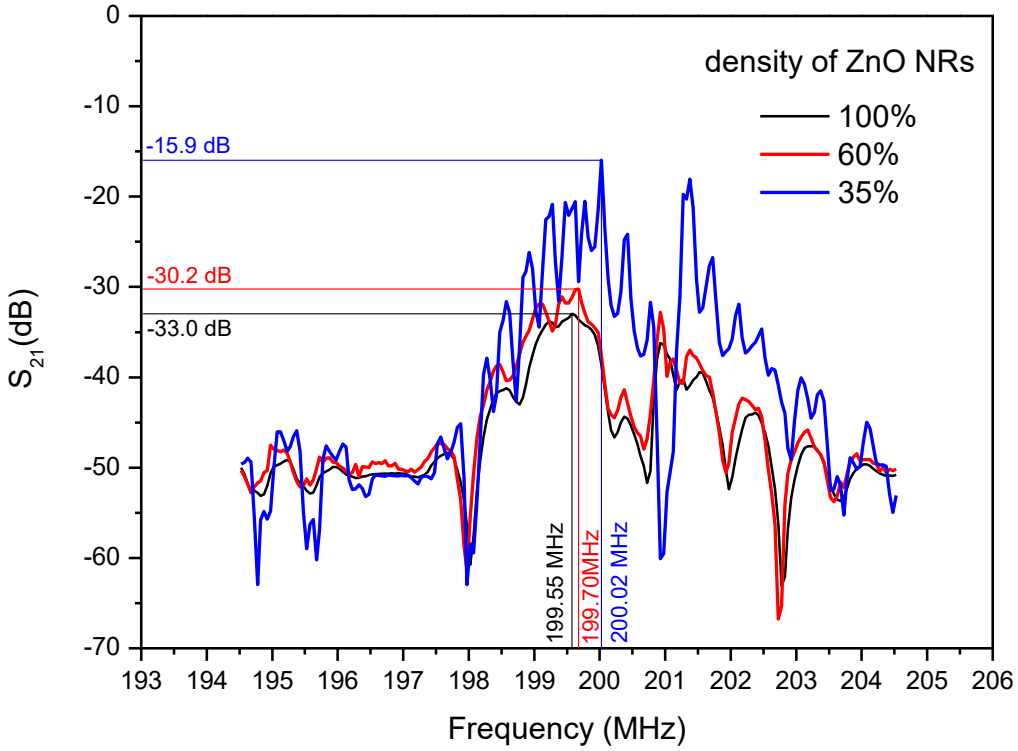
density of ZnO NRs
100%
60%
35%
-15.9 dB
-30.2 dB
-33.0 dB
199.55 MHz
199.70MHz
200.02 MHz
S21(dB)
Frequency (MHz)
0
-10
-20
-30
-40
-50
-60
-70
193
194
195
196
197
198
199
200
201
202
203
204
205
206

Fig.4

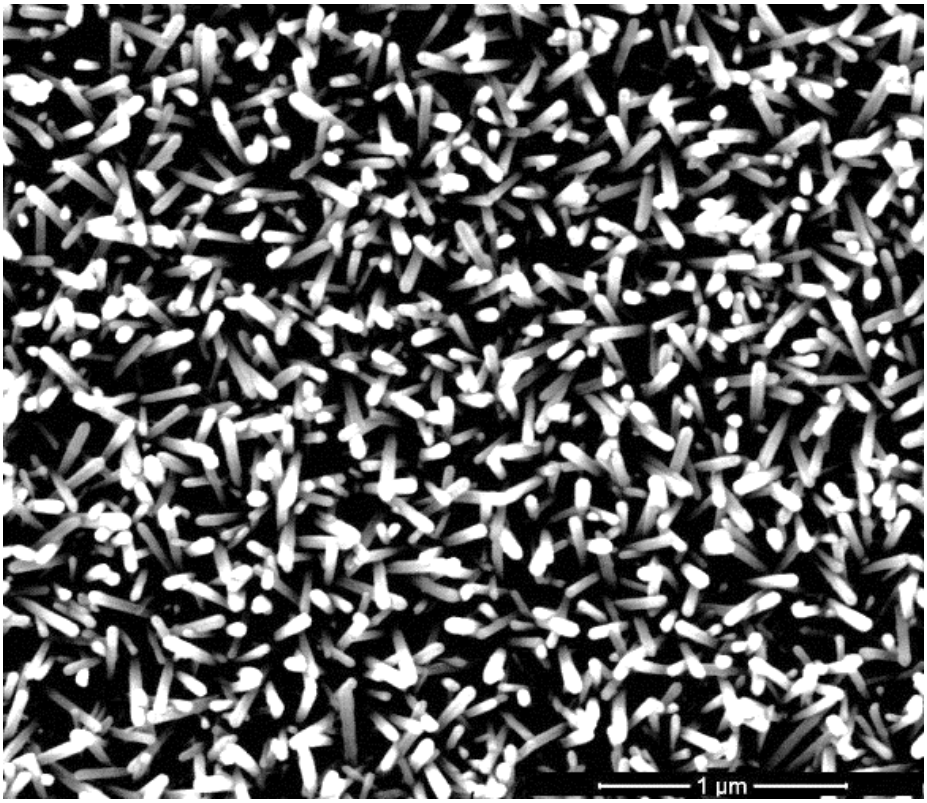

(a)

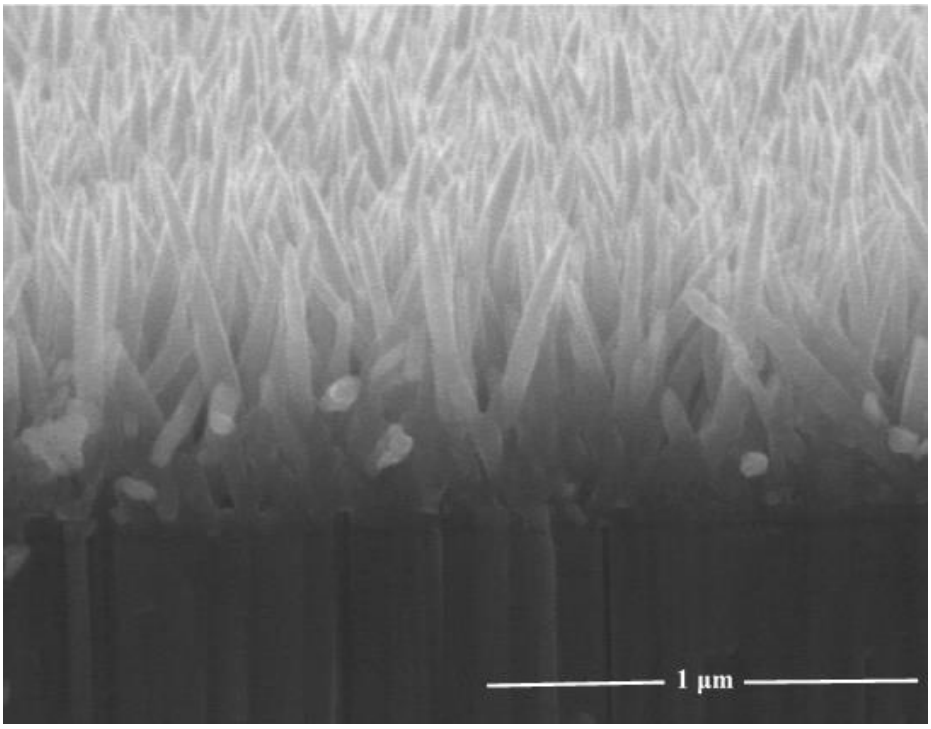

(b)

Fig.5

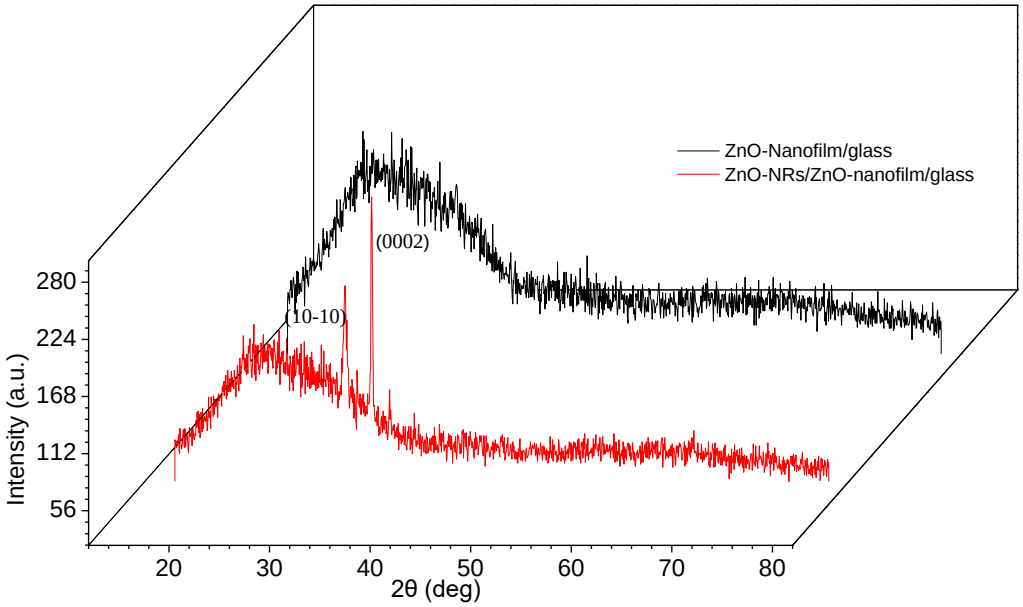
ZnO-Nanofilm/glass
ZnO-NRs/ZnO-nanofilm/glass
(0002)
(10-10)
Intensity (a.u.)
280
224
168
112
56
20
30
40
50
60
70
80
2θ (deg)

Fig.6

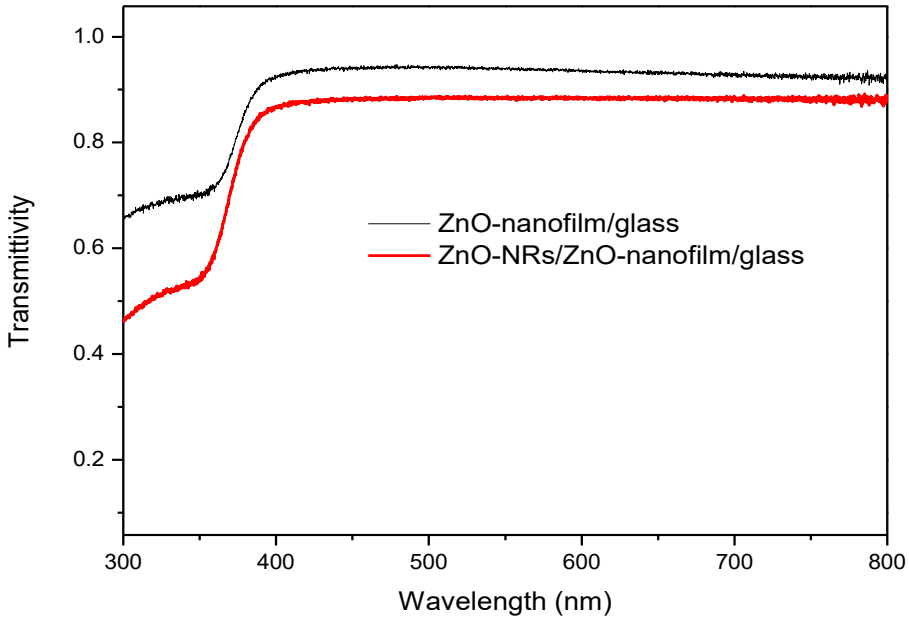
Transmittivity
1.0
0.8
0.6
0.4
0.2
300
400
500
600
700
800
Wavelength (nm)
ZnO-nanofilm/glass
ZnO-NRs/ZnO-nanofilm/glass

Fig.7

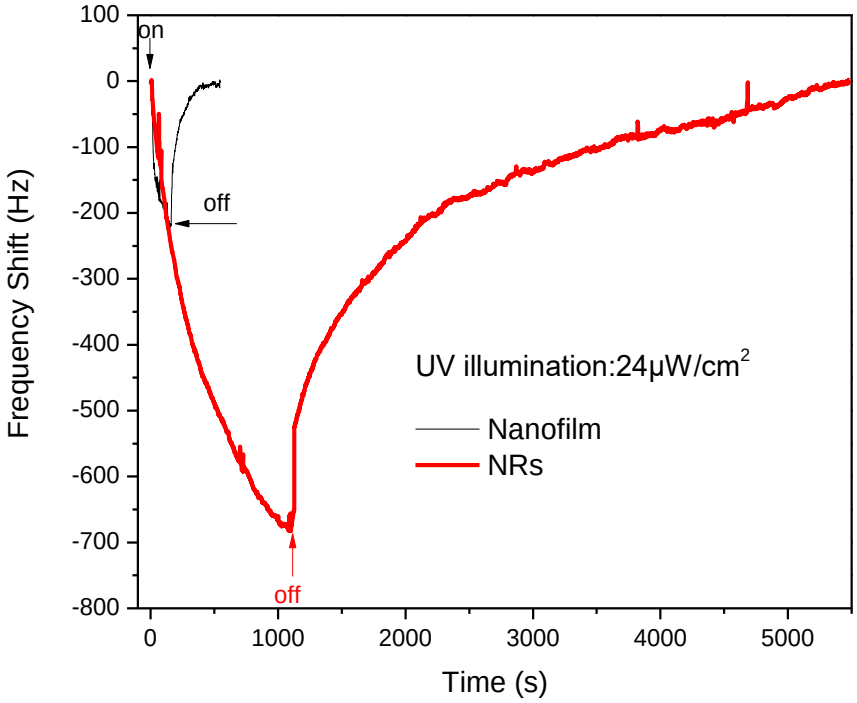
100
0
-100
-200
-300
-400
-500
-600
-700
-800
Frequency Shift (Hz)
on
off
off
UV illumination:24μW/cm2
Nanofilm
NRs
0
1000
2000
3000
4000
5000
Time (s)

Fig.8

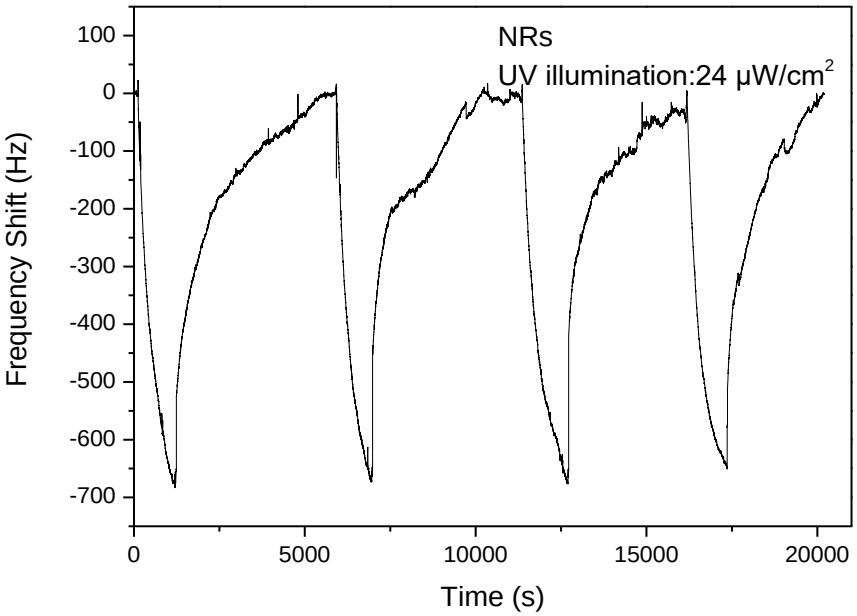
NRs
UV illumination:24 μW/cm2
Frequency Shift (Hz)
Time (s)
100
0
-100
-200
-300
-400
-500
-600
-700
0
5000
10000
15000
20000

(a)

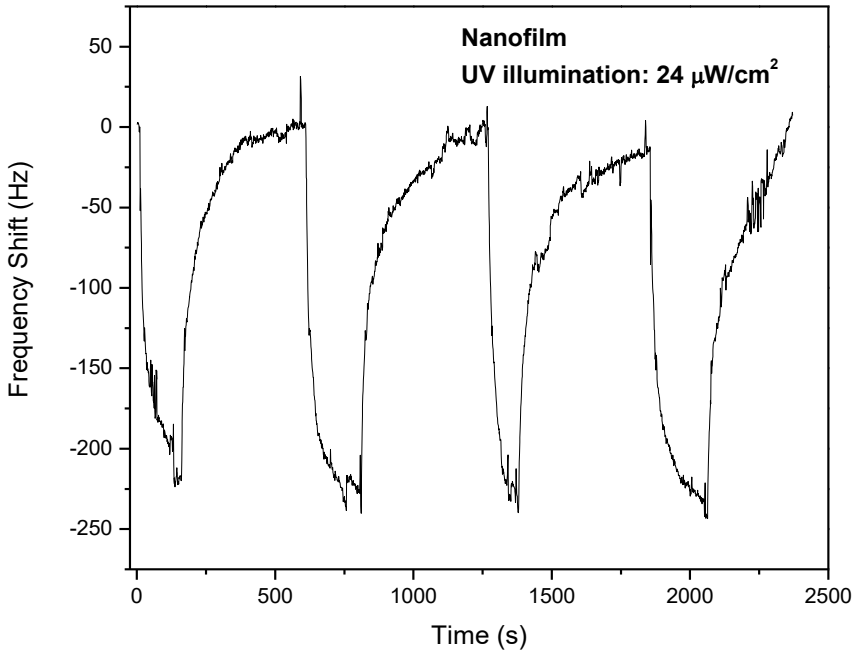
Nanofilm
UV illumination: 24 μW/cm2
Frequency Shift (Hz)
Time (s)
50
0
-50
-100
-150
-200
-250
0
500
1000
1500
2000
2500

(b)

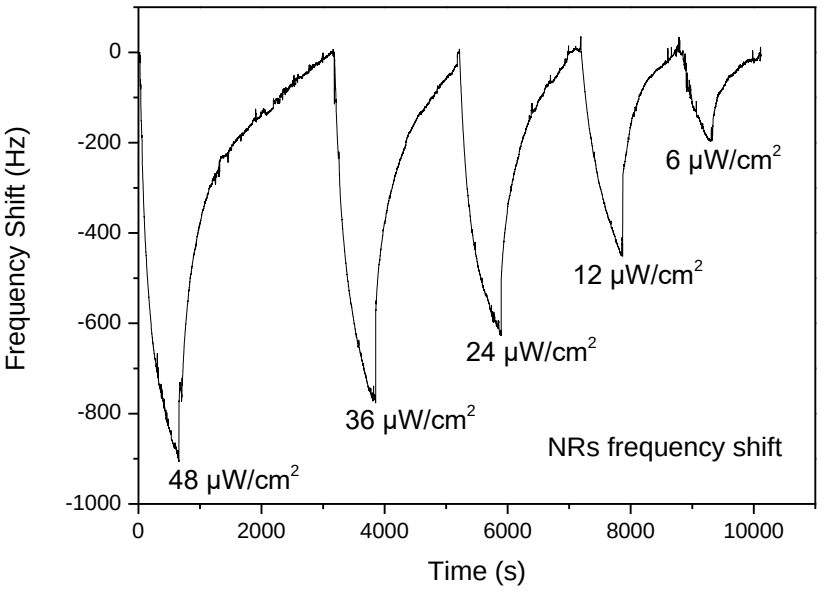
Frequency Shift (Hz)
0
-200
-400
-600
-800
-1000
0
2000
4000
6000
8000
10000
Time (s)
48 μW/cm2
36 μW/cm2
24 μW/cm2
12 μW/cm2
6 μW/cm2
NRs frequency shift

(c)

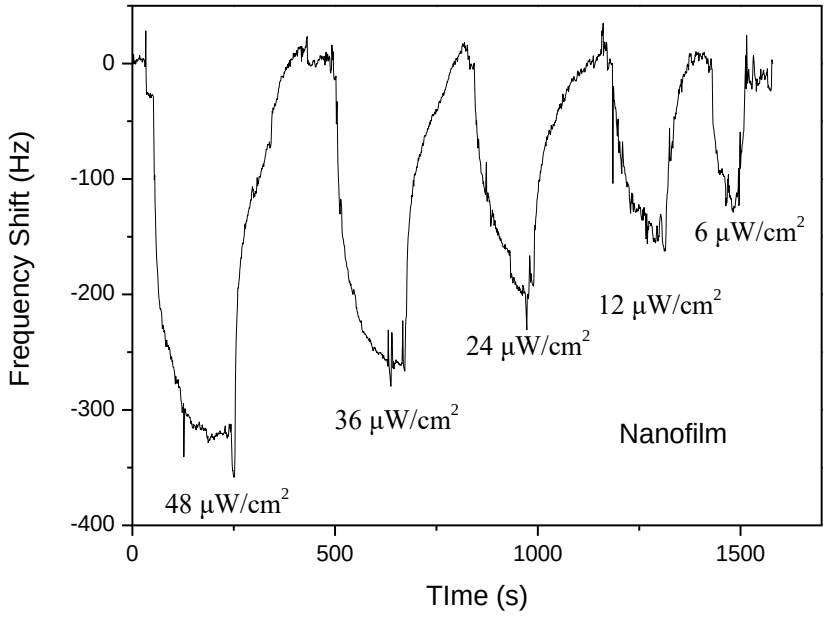
Frequency Shift (Hz)
0
-100
-200
-300
-400
0
500
1000
1500
TIme (s)
48 μW/cm2
36 μW/cm2
24 μW/cm2
12 μW/cm2
6 μW/cm2
Nanofilm

(d)

Fig.9

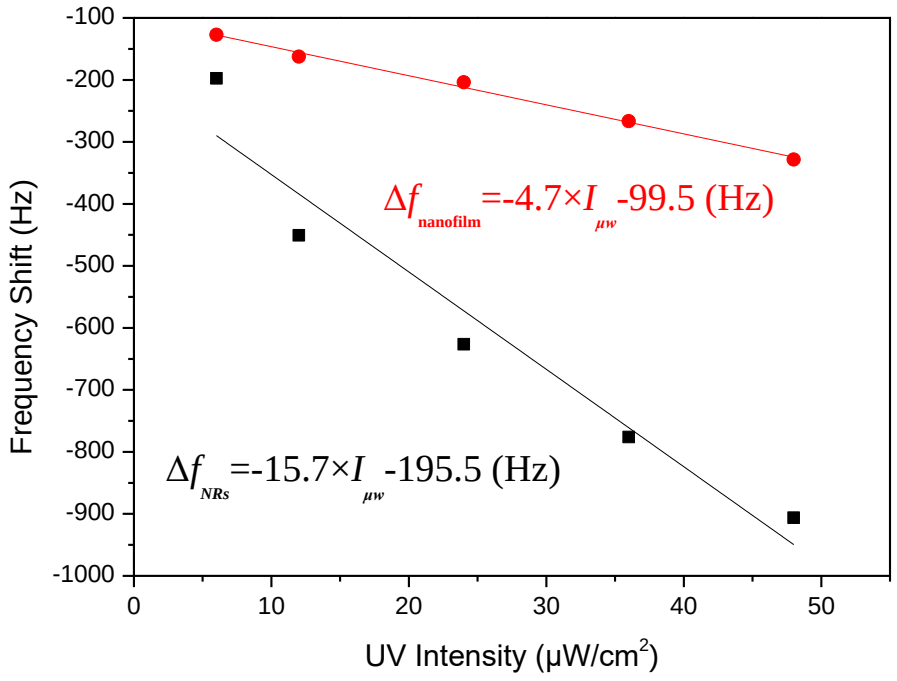

Fig.10

Table 1 Parameters of two-port ST-cut quartz SAW resonator devices.
Table 2 Sensing results of ZnO nanofilm and NRs to 365 nm UV light at a power density of 24 μW/cm^2.
Table 3 Sensing results of ZnO nanofilm and NRs to 365 nm UV light at different power densities.
Table 4 Comparisons of performance of reported UV light detectors based on SAW devices from literature and also from this study.

Table 1

Dimension (L×W×H)	12 mm×3 mm×0.5 mm
Number of fingers pairs	30
Number of grating fingers	100
Wavelength (λ =4 d)	16 μm
Aperture of IDTs	3 mm
Distance between IDTs	4 mm

Table 2

Frequency Shift（Hz）	ZnO nanofilm	ZnO NRs
Δf_1	-224	-683
Δf_2	-238	-673
Δf_3	-240	-676
Δf_4	-243	-651
Average Δf	-236	-671

Table 3

UV intensity ($\mu W/cm^2$)	ZnO nanofilm			ZnO NRs		
	Frequency response Shift (Hz)	response time (s)	recovery time (s)	Frequency response Shift (Hz)	response time (s)	recovery time (s)

6		-127	40	29
-198	400	575		
12		-163	107	42
-451	506	642		
24		-230	110	101
-626	514	807		
36		-266	155	115
-776	536	1012		
48		-328	90	168
-906	450	1787		

Table 4

Sensing layer	Substrate	Resonance mode	Resonant frequency (MHz)	Frequency shift (KHz)	UV intensity (mw/cm^2)	Sensitivity (ppm $(mw/cm^2)^{-1}$)
ZnO[a]	Quartz	Rayleigh	41.2	45	19	57.5
ZnO[b]	$LiNbO_3$	Rayleigh	37	170	40	114.9
ZnO[c]	Si	Rayleigh	122.15	10	3	27.3
ZnO[d]	Si	Rayleigh	180.7	12	0.6	110.7
ZnO[d]	Si	Sezawa	271.83	25	0.6	153.3
ZnO NRs[e]	Quartz	Rayleigh	200.02	0.9	0.048	93.7
ZnO[e]	Quartz	Rayleigh	200.08	0.3	0.048	31.3

[a] Reference [24]. [b] Reference [25]. [c] Reference [7]. [d] Reference [27]. [e] this work.